Nanoscale Advances

ROYAL SOCIETY OF CHEMISTRY

PAPER

View Article Online
View Journal | View Issue

Cite this: *Nanoscale Adv.*, 2023, **5**, 5385

Robust 2 nm-sized gold nanoclusters on Co_3O_4 for CO oxidation†

Quanquan Shi,*[ae] Zhiwen Li,[bd] Changhai Cao,[c] Gao Li *[bd] and Sami Barkaoui*[b]

Received 26th July 2023
Accepted 5th September 2023

DOI: 10.1039/d3na00561e

rsc.li/nanoscale-advances

In this study, gold nanoparticles were dispersed on Co_3O_4 nanoplates, forming a specific Au–Co_3O_4 interface. Upon calcination at 300 °C in air, aberration-corrected STEM images evidenced that the gold nanoclusters (NCs) on Co_3O_4{111} were maintained at *ca.* 2.2 nm, which is similar to the size of the parent Au colloidal particles, demonstrating the stronger metal-support interaction (SMSI) on Co_3O_4{111}. Au/Co_3O_4{111} showed good catalytic activity (a full CO conversion achieved at 80 °C) and durability (over 10 hours) in CO oxidation, which was mainly due to the promotion by the surface oxygen vacancies and intrinsic defects of Co_3O_4{111} for activating O_2 and by Au^0, $Au^{\delta+}$, and Au^+ species on the surface of gold NCs for CO activation, as evidenced by Raman and Fourier-transform infrared (FT-IR) spectroscopy analysis. Au/Co_3O_4 catalyzed CO oxidation obeyed the Langmuir–Hinshelwood mechanism at low temperatures.

Introduction

Carbon monoxide (CO), emitted from mobile and stationary combustion sources, is one of the major air pollutants, and its presence even in traceable amounts may cause serious environmental and health problems. Therefore, the elimination of CO, *via* oxidation by air, acts as one of the important technologies for air cleanup. Gold nanoparticles (NPs) at the size range of 2–5 nm, supported on reducible oxides, have been demonstrated to be extremely active for CO oxidation even at room temperature.[1,2] However, the chemical nature of gold particle sizes and the identification of active sites is still being debated. There are several parameters, including the chemical state of Au, the size of the Au-NPs, and the gold–support interface, that can intensely affect the activity of CO oxidation on gold catalysts.[3–7] To date, the interfacial perimeter of the Au NPs and oxide supports is popularly proposed as the active site for CO oxidation, where the reaction occurs *via* a redox mechanism. For example, on Au/TiO_2 (ref. 4 and 5) and Au/Fe_2O_3,[7] CO is proposed to be chemically adsorbed on gold NPs and the O_2 gas is activated on the oxygen vacancy at the interface. Therefore, identification of the atomic structure of the active gold-oxide is of critical importance for the design of highly active gold catalysts. The geometrical structure of the gold-supported interface at the atomic scale is less studied.

Reducible oxides, such as Fe_2O_3, TiO_2, CeO_2, and Co_3O_4, often exhibit exceptionally high activity for CO oxidation, when they are used to support gold nanoparticles.[8–14] This is primarily because these oxides could create oxygen vacancies on their surfaces close to the Au particles, forming strong metal-support interactions (SMSI). In this context, Au/Co_3O_4 catalyst has attracted particular attention because of their exceptionally high activities for low-temperature CO oxidation.[15] The key function of cobalt oxide is to disperse and stabilize gold NPs through its surface oxygen vacancies that strongly depend on the size and shape of cobalt oxide crystallites. The dispersion of gold NPs on high surface area support is expected to promote catalytic activity and stability, as it not only increases the gold loading but also improves its dispersion, which would be beneficial to avoid the sintering of Au NPs.[16,17]

Herein, we prepared a nanoplate-shaped Co_3O_4 oxide with the preferential exposure of Co_3O_4{111} as the support to disperse gold nanoclusters (NCs) with a uniform size of ~2 nm. The atomic arrangements of Au{111} were obtained by aberration-corrected STEM technology, which formed a strong metal-support interaction. The resulting Au/Co_3O_4 catalysts, exhibiting surface oxygen vacancies and intrinsic defects of Co_3O_4{111} and the Au^0, $Au^{\delta+}$, and Au^+ species on the surface of gold NCs, showed significant activities in the CO oxidation at low reaction temperatures. The catalyzed CO

[a]College of Science, Inner Mongolia Agricultural University, Hohhot 010018, China. E-mail: qqshi@imau.edu.cn

[b]State Key Laboratory of Catalysis, Dalian Institute of Chemical Physics, Chinese Academy of Sciences, Dalian 116023, China. E-mail: gaoli@dicp.ac.cn; samibarkaoui501@gmail.com

[c]Key Laboratory of Biofuels and Biochemical Engineering, SINOPEC Dalian Research Institute of Petroleum and Petrochemicals Co., Ltd, Dalian 116045, China

[d]University of Chinese Academy of Sciences, Beijing 100049, China

[e]Inner Mongolia Key Laboratory of Soil Quality and Nutrient Resource & Key Laboratory of Agricultural Ecological Securi-ty and Green Development at Universities of Inner Mongolia Autonomous, Hohhot 010018, China

† Electronic supplementary information (ESI) available. See DOI: https://doi.org/10.1039/d3na00561e

oxidation over Au/Co_3O_4 obeyed the Langmuir–Hinshelwood mechanism at low temperatures.

Experimental

Synthesis of Co_3O_4 oxides

Co_3O_4 was synthesized following typical procedures reported in the literature.[18,19] $CoCl_2 \cdot 6H_2O$ was dissolved in deionized water, and triethylamine was added. After 10 min stirring, the solution was transferred and reacted at 180 °C for 20 h in an autoclave. The precipitates were filtered and washed with deionized water, followed by calcination at 350 °C for 3 h, which was then used to support the gold particles.

Preparation of Au/$_{Co3O4}$ catalysts

Au/Co_3O_4 catalysts were prepared by an immobilization method of Co_3O_4 oxides with Au:PVP (polyvinyl alcohol) colloids of ~2 nm, which were prepared by a typical procedure.[7] Typically, Co_3O_4 oxides were added into the aqueous solution containing the fresh Au:PVP colloids, which were stirred at room temperature for 3 h. The solid was collected by filtration and washed with distilled water. The solid sample was dried at 80 °C and calcined at 300 °C for 2 h in air to remove all the PVP ligands. Furthermore, the analysis of inductively coupled plasma mass spectroscopy (ICP-MS) showed that the actual loading of Au was 0.65 wt% in the prepared Au/Co_3O_4.

Characterization

X-ray powder diffraction patterns were recorded on a Rigaku D/MAX-2500PC with Cu Kα radiation (λ 1.5418 Å) at 40 kV and 200 mA. Transmission electron microscopy (TEM) images were recorded on a Hitachi 7700 microscope operated at 120 kV. Aberration-corrected scanning transmission electron microscopy (AC-STEM) images were obtained on a JEM-ARM200F at 200 kV. The specimen was prepared by ultrasonically dispersing the sample powder into ethanol, and drops of the suspension were deposited on a carbon-coated copper grid and dried at room temperature. Raman spectra were collected using a Renishaw inVia Raman microscope with a laser wavelength of 785 nm and a laser power of 3 mW and were taken under the same conditions after 60 seconds of exposure. TPO analysis was performed with an AutoChem II 2920 instrument (Micromeritics) and analyzed with a thermal conductor detector (TCD). Before analysis, 50 mg of the samples were pre-treated at 200 °C for 1 h in He gas to clean the surface of the samples. After cooling to room temperature, 5% of O_2/He (30 mL min^{-1}) was used as a feed gas to perform TPO from RT to 600 °C. The infrared Fourier transform spectra were recorded using a Vertex 70v spectrometer (Bruker). Spectra were recorded at 4 cm^{-1} spectral resolution and 60 kHz scanning velocity. Au/Co_3O_4 samples were pretreated at 300 °C in an Ar atmosphere for one hour. After the system was cooled to room temperature, the flow was switched to a feed gas of 1% CO/Ar, and the infrared spectra were *in situ* recorded. Visible Raman spectra were collected on a Jobin-Yvon U1000 scanning double monochromator with a 532 nm single-frequency laser.

Catalytic test

CO oxidation was performed in a flow reactor. Preliminary reactions were carried out with ~0.200 g Au/Co_3O_4 or pristine Co_3O_4 catalysts were taken in the form of 40–60 mesh particles. Before the reactions, the samples were activated at 300 °C for 1 h in the presence of 20% O_2/N_2 gas. When the reactor was cooled to room temperature, a feed gas (1% CO/20% O_2/N_2) was passed over the catalysts at a flow rate of 30 mL min^{-1}. The amounts of CO, CO_2, and O_2 in the inlet and outlet streams were analyzed using an online gas chromatograph. The CO conversion (X_{CO}, %) was calculated on the basis of CO consumption and CO_2 formation by eqn (1):

$$X_{CO} = (C_0 - C_1)/C_0 \times 100\% \quad (1)$$

where, C_0 and C_1 represent the CO concentrations at the inlet and outlet of the reactor, respectively.

Results and discussion

Characterization of Au/Co_3O_4

The XRD pattern of the as-prepared Au/Co_3O_4 catalyst is shown in Fig. 1. The diffraction peaks of Co_3O_4 were observed at 19.0°, 31.3°, 36.8°, 44.8°, 55.7°, 59.4°, and 65.2°, which can be assigned to the (111), (220), (311), (222), (400), (422), (511), and (440) planes of the Co_3O_4 phase (JPDS No. 00-042-1467), respectively, with a space group of *Fd3m*.[20] The high peak intensities confirmed the high crystallization of the Co_3O_4 support. Another XRD peak at ~38.5° corresponds to the Au(111) phase, clearly suggesting the existence of gold NCs in the Au/Co_3O_4 sample.[21]

Furthermore, the morphology of gold NCs and Co_3O_4 oxides and the size of Au particles were characterized by TEM methods. TEM images showed that the Co_3O_4 oxide had a hexagonal shape, with an average edge length of ~160 nm and thickness of ~25 nm. As shown in the AC-STEM image, Au NCs of the Au/Co_3O_4 showed a particle size of 2.2 ± 0.6 nm (Fig. 2a). Au particles were uniformly loaded onto the surface of the Co_3O_4{111} plane, based on the lattice fringes with an interplanar spacing of 0.46 nm, which can be attributed to the Co_3O_4{111} of Co_3O_4 (Fig. 2b).[18,22]

To study the chemical state of the surface gold atoms on the gold nanoparticles, Fourier-transform infrared (FT-IR)

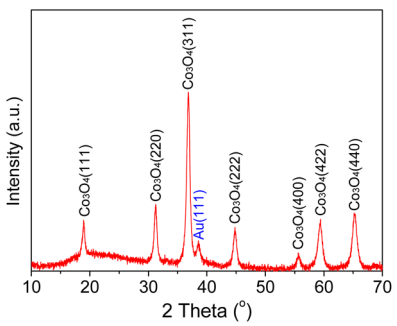

Fig. 1 Powder XRD of the Au/Co_3O_4 sample.

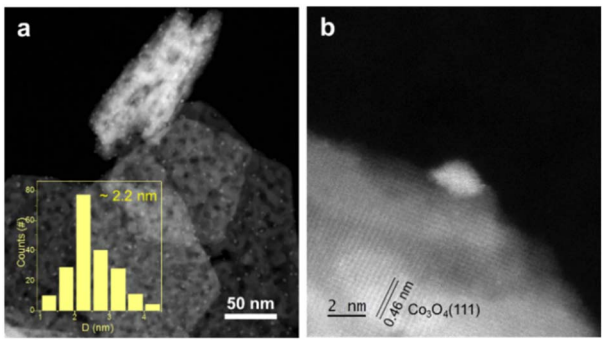

Fig. 2 (a) AC-STEM images of Au/Co_3O_4 sample. (b) The Au particle on Co_3O_4{111}. Statistics in (a) were performed by counting 202 particles.

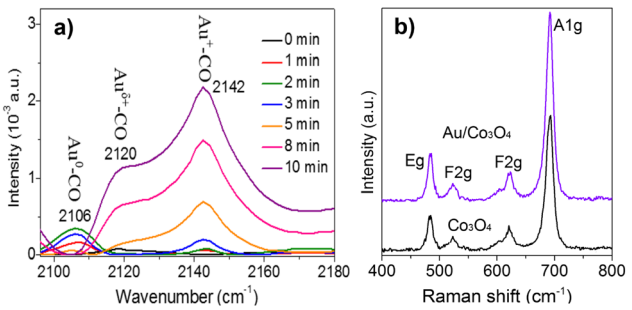

Fig. 3 (a) CO-FTIR of Au/Co_3O_4 catalysts. The adsorption bands at 2105 cm^{-1}, 2120 cm^{-1}, and 2142 cm^{-1} are assigned to the Au^0–CO, $Au^{\delta+}$–CO ($0 < \delta < 1$), and Au^+-CO species, respectively. (b) Raman spectra of the bare Co_3O_4 oxides and the as-prepared Au/Co_3O_4 catalysts.

spectroscopy for the CO adsorption on the Au/Co_3O_4 catalyst was employed at room temperature. As shown in Fig. 3a, the CO adsorption on Au/Co_3O_4 results in the appearance of three bands in the carbonyl stretching region, with their maxima located at 2106 cm^{-1}, 2120 cm^{-1}, and 2142 cm^{-1}. The adsorption band at 2106 cm^{-1} is assigned to CO absorbed linearly on metallic gold particles (Au^0–CO).[23,24] It can be predicted that this band characterizes weakly adsorbed species because it easily disappeared even after a short time of 2 min. The band observed at 2120 cm^{-1} can be attributed to $Au^{\delta+}$–CO ($0 < \delta < 1$). The 2142 cm^{-1} band frequency region can be assigned to CO adsorbed on gold exposed at the surface of the particles where gold sites are to some extent, made electropositive by the adsorbed oxygen (Au^+–CO).[23] Thus, $Au^{\delta+}$ and Au^+ species coexist on the surface of the gold particles, which facilitates the nanogold-catalyzed CO oxidation for the adsorption and activation of CO molecules.

Furthermore, Raman analysis was carried out to clearly identify the surface oxygen vacancies of the bare Co_3O_4 oxides and Au/Co_3O_4 catalyst. As presented in Fig. 3b, the bare Co_3O_4 and Au/Co_3O_4 displayed similar Raman features: four vibration peaks (*i.e.*, $A_{1g} + E_g + 2\ F_{2g}$) in the range of 400–800 cm^{-1}. The Raman peaks at 484 cm^{-1}, 523 cm^{-1}, and 622 cm^{-1} are assigned to the E_g, $F2g^{(2)}$, and $F_{2g}^{(1)}$ symmetry, respectively. Another peak at 691 cm^{-1} with A_{1g} symmetry is attributed to the characteristics of the octahedral CoO_6 sites, corresponding to the unique characteristics of the spinel-type cubic Co_3O_4 phase, in good agreement with the reported literature[25,26] Furthermore, the ratio of the surface oxygen vacancies to surface lattice oxygen was calculated to be 0.46 on the Co_3O_4 support and 0.52 ion Au/Co_3O_4, based on the full width at half-maximum of A_{1g} peaks.[25] Thus, Au/Co_3O_4 exhibits obviously high defective structures, induced by the anchored Au nanoclusters, which can promote the oxidation, as the defective structures can largely promote the adsorption and activation of oxygen species during the catalytic CO oxidation.[27]

Catalytic performance

Furthermore, Au/Co_3O_4 catalysts were evaluated in the CO oxidation reactions. As shown in Fig. 4a, the bare Co_3O_4 oxide

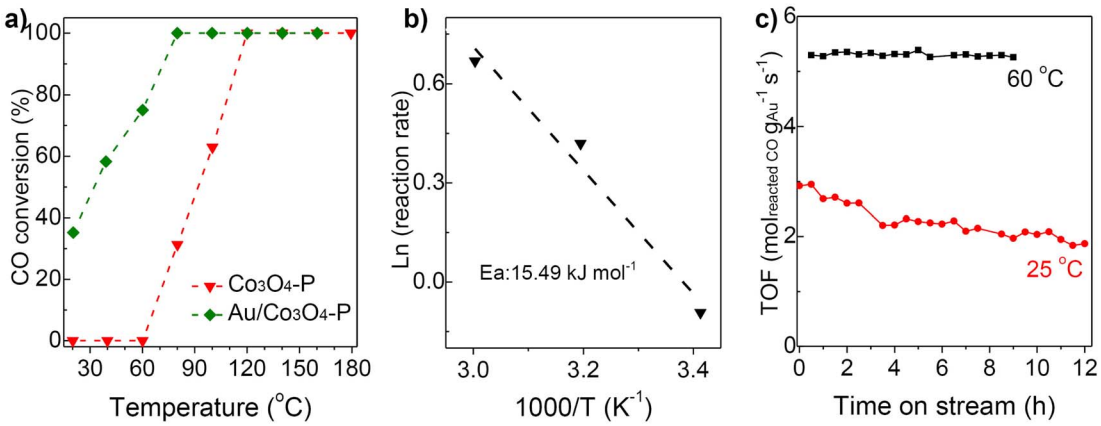

Fig. 4 (a) Catalytic activity of Co_3O_4 oxides and Au/Co_3O_4 for CO oxidation as the function of temperature. Reaction conditions: the gas flow was composed of 1% CO/20% O_2/N_2 (vol.) with a flow rate of 30 mL min^{-1}, and 50 mg catalysts were used. (b) Arrhenius plots of the rate *vs.*(1/*T*) for CO oxidation reaction over Au/Co_3O_4 catalysts. (c) Durability tests of Au/Co_3O_4 catalysts in the CO oxidation at 25 °C (using 50 mg of catalyst) and 60 °C (40 mg of catalyst). Tests conditions: 1% CO/20% O_2/N_2 with a flow rate of 30 mL min^{-1}. The CO conversion were measured in the range of 25% to 45%.

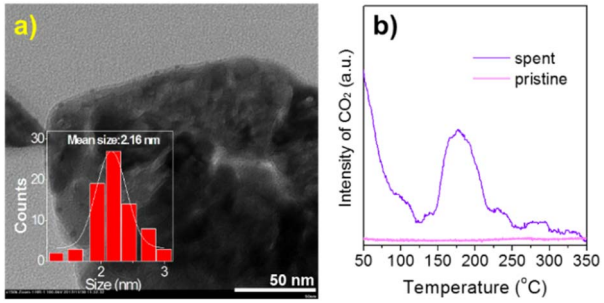

Fig. 5 (a) TEM image and (b) TPO analysis of the spent Au/Co_3O_4 after CO oxidation. The statistical analysis was performed by counting over 100 gold particles.

was inactive at low reaction temperatures of 20–60 °C and showed a 31% CO conversion at 80 °C and a full conversion at 120 °C. While, the Au/Co_3O_4 catalyst gave a promising CO conversion (35%) at a low temperature of 20 °C, and the full CO conversion was achieved at 80 °C, Fig. 4a, green line. Therefore, the introduction of Au NCs largely promoted the catalytic activity in CO oxidation. The activation energy for CO oxidation was calculated to be 15.49 kJ mol^{-1} for Au/Co_3O_4, in good agreement with that reported in the early literature.[28] Therefore, we deduce that the Au/Co_3O_4-catalyzed CO oxidation should obey the Langmuir–Hinshelwood mechanism at low temperatures (20–60 °C), as the oxygen molecules and CO should be adsorbed and activated over the surface oxygen vacancies and gold particles, respectively, rather than on the surface lattice oxygen sites.[29,30]

Furthermore, the durability of the Au/Co_3O_4 catalysts was investigated at 25 and 60 °C. As depicted in Fig. 4c, the activity of the Au/Co_3O_4 catalysts was dropped from 2.92 to 1.87 $mol_{reacted\ CO}\ g_{Au}^{-1}\ s^{-1}$ during the 12 h reaction in the CO oxidation (red line). While, Au/Co_3O_4 gave a stable activity performance of 5.26–5.39 $mol_{reacted\ CO}\ g_{Au}^{-1}\ s^{-1}$ during the test (9 h, black line), which is higher than the reported value over the oxide-supported gold NCs catalysts, as shown in Table S1.†[8–12] Overall, the results indicated that Au/Co_3O_4 catalysts exhibited excellent durability for CO oxidation. No apparent sintering of Au NCs was observed in TEM analysis of the spent Au/Co_3O_4 catalysts (Fig. 5a), demonstrating that the slight activity loss was not caused by the aggregation of gold particles. The CO_2 species were clearly observed in the TPO tests of the spent Au/Co_3O_4 catalysts, compared with the pristine one, as shown in Fig. 5b. Hence, the slight deactivation at low reaction temperature (*e.g.*, 25 °C) should be associated with the formation and accumulation of carbonate-like and H_2O/OH^- species at the support interface, resulting in the blockage of active sites during the CO oxidation reaction.[31–34]

Conclusions

In summary, gold nanoclusters of *ca.* 2.2 nm immobilized on the nanoplate-shaped Co_3O_4 oxides were synthesized by a simple impregnation of gold colloids and oxides. STEM analysis identified that the Au particles of Au{111} and Au{100} exposures interacted with Co_3O_4{111}. Au/Co_3O_4{111} exhibited good catalytic activity and durability in the CO oxidation, which may be due to the strong metal-support interaction. FT-IR and Raman spectroscopy analyses confirmed that the surface oxygen vacancies and intrinsic defects on Co_3O_4{111} and $Au^{\delta+}$ and Au^+ species on the surface of gold NCs are responsible for the high catalytic behavior in the CO oxidation.

Conflicts of interest

There are no conflicts to declare.

Acknowledgements

We thank the financial support from the fund of National Natural Science Foundation of China (22065029 and 22172167), the Natural Science Foundation of Inner Mongolia Autonomous Region (2022MS02002), and central guidance for Local Scientific and Technological Development funds (2022ZY0081).

Notes and references

1 G. C Bond and D. T. Thompson, *Catal. Rev.: Sci. Eng.*, 1999, **41**, 319–388.
2 Z. Li, X. Zhang, Q. Shi, X. Gong, H. Xu and G. Li, *Nanoscale Adv.*, 2021, **3**, 7002–7006.
3 Z. Jin, Y. Y. Song, X. P. Fu, Q. S. Song and Ch.-J. Jia, *Chin. J. Chem.*, 2018, **36**, 639–643.
4 X. Wei, B. Shao, Y. Zhou, Y. Li, Ch. Jin, J. Liu and W. Shen, *Angew. Chem.*, 2018, **57**, 11289–11293.
5 X. Du, Y. Huang, X. Pan, B. Han, Y. Su, Q. Jiang, M. Li, H. Tang, G. Li and B. Qiao, *Nat. Commun.*, 2020, **11**, 5811.
6 Y. Wang, D. Widmann, F. Lehnert, D. Gu, F. Schuth and R. Jurgen Behm, *Angew. Chem.*, 2017, **56**, 1–7.
7 B. Shao, J. Zhang, J. Huang, B. Qiao, Y. Su, Sh. Miao, Y. Zhou, D. Li, W. Huang and W. Shen, *Small Methods*, 2018, **2**, 1800273.
8 Y. Zhang, Z. Li, J. Zhang, L. Xu, Z. Han, A. Baiker and G. Li, *Nano Res.*, 2023, **16**, 8919–8928.
9 M. Chen and D. W. Goodman, *Acc. Chem. Res.*, 2006, **39**, 739–746.
10 A. A. Herzing, C. J. Kiely, A. F. Carley, P. Landon and G. J. Hutchings, *Science*, 2008, **321**, 1331–1335.
11 W. Li, C. Liu, H. Abroshan, Q. Ge, X. Yang, H. Xu and G. Li, *J. Phys. Chem. C*, 2016, **120**, 10261–10267.
12 Y. Denkwitz, Z. Zhao, U. Hormann, U. Kaiser, V. Plzak and R. J. Behm, *J. Catal.*, 2007, **251**, 437–442.
13 Z. Li, W. Li, H. Abroshan, Q. Ge, Y. Zhou, C. Zhang, G. Li and R. Jin, *Nanoscale*, 2018, **10**, 6558–6565.
14 H. Atout, A. Bouguettouch, D. Chebli, J. Crespo, J. Dupin, J. M. López-de-Luzuriaga, H. Martínez, M. Monge, M. Elena Olmos and M. Rodríguez-Castillo, *New J. Chem.*, 2021, **45**, 11727–11736.
15 Z. Zhou, S. Kooi, M. Flytzani-Stephanopoulos and H. Saltsburg, *Adv. Funct. Mater.*, 2008, **18**, 2801–2807.
16 Y. Liu, H. Dai, J. Deng, S. Xie, H. Yang, W. Tan, Y. Jiang and G. Guo, *J. Catal.*, 2014, **309**, 408–418.

17 Q. Shi, X. Zhang, Z. Li, A. Raza and G. Li, *ACS Appl. Mater. Interfaces*, 2023, **15**, 30161–30169.
18 T. Barakat, J. C. Rooke, E. Genty, R. Cousin, S. Siffert and B. I. Su, *Energy Environ. Sci.*, 2013, **6**, 371–391.
19 X. Wei, S. Barkaoui, J. Chen, Q. Fang, G. Cao, Z. Wu, F. Wang and G. Li, *Nanoscale Adv.*, 2021, **3**, 1741–1746.
20 U. Sengupta, A. Mukherjee, M. P. S. Mukhopadhyay, K. J. Jenkinson, A. E. H. Wheatley and A. Kar, *New J. Chem.*, 2023, **47**, 11425–11443.
21 Y. Guo, Q. Zhou, X. Chen, Y. Fu, S. Lan, M. Zhu and Y. Du, *J. Mater. Sci. Technol.*, 2022, **119**, 53–60.
22 H. Chen, M. Yang, S. Tao and G. Chen, *Appl. Catal., B*, 2017, **209**, 648–656.
23 F. Boccuzzi, A. Chiorino and M. Manzoli, *Surf. Sci.*, 2000, **454–456**, 942–946.
24 X. Zhang, Z. Li, W. Pei, G. Li, W. Liu, P. Du, Z. Wang, Z. Qin, H. Qi, X. Liu, S. Zhou, J. Zhao, B. Yang and W. Shen, *ACS Catal.*, 2022, **12**, 3634–3643.
25 G. Zhai, J. Wang, Z. Chen, W. An and Y. Men, *Chem. Eng. J.*, 2018, **337**, 488–498.
26 S. Barkaoui, M. Haddaoui, H. Dhaouadi, N. Raouafi and F. Touati, *J. Solid State Chem.*, 2015, **228**, 226–231.
27 Y. Cao, L. Zhao, T. Gutmann, Y. Xu, L. Dong, G. Buntkowsky and F. Gao, *J. Phys. Chem. C*, 2018, **122**, 20402–20409.
28 M. Haruta, S. Tsubota, T. Kobayashi, H. Kageyama, M. J. Genet and B. Delmon, *J. Catal.*, 1993, **144**, 175–192.
29 Y. Chen, Y. Li, W. Chen, W. Xu, Z. Han, A. Waheed, Z. Ye, G. Li and A. Baiker, *Nano Res.*, 2022, **15**, 1366–1374.
30 Y. Wang, Q. Jiang, L. Xu, Z. Han, S. Guo, G. Li and A. Baiker, *ACS Appl. Mater. Interfaces*, 2021, **13**, 61078–61087.
31 H. Wang, H. Zhu, Z. Qin, F. Liang, G. Wang and J. Wang, *J. Catal.*, 2009, **26**, 154–162.
32 C. H. Kim and L. T. Thompson, *J. Catal.*, 2005, **230**, 66–74.
33 Q. Guo, S. Chen, Y. Liu and Y. Wang, *Chem. Eng. J.*, 2010, **165**, 846–850.
34 Q. Shi, Y. Zhang, Z. Li, Z. Han, L. Xu, A. Baiker and G. Li, *Nano Res.*, 2023, **16**, 6951–6959.